Nanoindentation of Phase-Specific Elastic Modulus in Virgin and Recycled HDPE Wood–Plastic Composites

Aldo Ballerini,[a,c] Pablo Moreno,[b,*] Paulina Valenzuela,[a] Jorge Chavez,[d] and William Gacitúa [a,c]

The structural behavior of natural fiber-reinforced polymer composites depends largely on the efficiency of stress transfer at the fiber–matrix interface. However, accurate determination of the interface thickness and its mechanical properties remains challenging in such materials. This study aimed to characterize the interface thickness and evaluate the elastic modulus of composites produced with virgin and recycled high-density polyethylene (HDPE) matrices. Nanoindentation was employed to determine the elastic modulus of each composite phase (wood fiber, interface, and matrix) individually, through sequential indentations performed across the wood fiber-interface-matrix regions. The mean elastic modulus values for the wood fiber, interface, and matrix in the 20/80 composite (20% wood fibers and 80% virgin HDPE) were 7.51, 6.17, and 2.26 GPa, respectively. For the recycled HDPE composite, the corresponding values were 8.16, 5.82, and 1.86 GPa. The mean interface thickness was 2.5 μm in the virgin-matrix composite and 0.63 μm in the recycled-matrix composite. These results demonstrate that the recycling of the polymer matrix influences both the interfacial structure and the local mechanical performance of natural fiber reinforced composites.

DOI: 10.15376/biores.21.2.2980-3001

Keywords: Nanoindentation; Interface thickness; Elastic modulus; Recycled HDPE; Natural fiber composites; Fiber–matrix interaction

*Contact information: a: Department of Process Engineering and Bioproducts, Faculty of Engineering, University of Bío-Bío, Collao 1202, P.O. Box 5-C, Concepción 4030000, Chile; b: Construction Technology Research Center (CITEC), University of Bío-Bío, Collao 1202, P.O. Box 5-C, Concepción 4030000, Chile; c: Biomass and Bioproducts Valorization Group, Faculty of Engineering, University of Bío-Bío, Collao 1202, P.O. Box 5-C, Concepción 4030000, Chile; d: Maderas Arauco Company, Continuous Improvement Department, Cholguán Complex, Yungay 3920000, Concepción, Chile; *Corresponding author: pmoreno@ubiobio.cl*

INTRODUCTION

Wood plastic composites (WPCs) are hybrid materials that combine wood fibers with polymeric matrices, offering an attractive balance between performance and sustainability. Their use has expanded in numerous applications due to environmental benefits such as the incorporation of recycled polymers, reduced deforestation, improved durability, lower chemical consumption, and decreased carbon emissions. The integration of natural and synthetic components enhances mechanical performance while promoting sustainable resource management.

The physical and mechanical properties of WPCs depend primarily on the interaction between the wood fibers and the polymer matrix. This interaction is influenced by the chemical nature, morphology, and proportion of each component, as well as by processing parameters that govern the formation of interfacial bonds (Isaza *et al.* 2022).

Key challenges in wood–plastic composites arise from the intrinsic incompatibility between hydrophilic lignocellulosic fibers and hydrophobic polyolefins. This mismatch results in weak interfacial adhesion, poor stress transfer, fiber pull-out, and suboptimal mechanical performance (Stark and Rowlands 2003). Compatibilizers such as maleated polyethylene (MAPE) are therefore widely employed to enhance the interfacial bonding between the polymer matrix and wood fibers. MAPE contains maleic anhydride groups capable of reacting with hydroxyl functionalities on the fiber surface, forming ester linkages or strong hydrogen-bonding interactions, while its polyethylene backbone remains miscible with the HDPE matrix. This dual affinity improves wetting, reduces interfacial voids, increases load-transfer efficiency, and leads to higher stiffness and strength at the composite scale (Beg and Pickering 2008). Moreover, improved interfacial adhesion can strongly influence local mechanical properties, making MAPE particularly relevant when evaluating the interphase by nanoindentation, where subtle changes in stiffness and deformation behavior can be directly measured at the micrometer scale (Eder *et al.* 2013).

In parallel with the increasing use of wood–plastic composites, the recycling of commodity polyolefins such as high-density polyethylene (HDPE) has become a key strategy to reduce the environmental footprint of these materials. Post-industrial and post-consumer HDPE streams are increasingly incorporated into new products; however, repeated extrusion and thermo-mechanical processing promote chain scission and oxidative degradation, resulting in reductions in molecular weight and crystallinity, slight decreases in melting temperature, and marked changes in melt flow index and rheological behavior (Cestari *et al.* 2014; Dou and Rodrigue 2021; Vidakis *et al.* 2021; Langwieser *et al.* 2022; Zhang and Rodrigue 2023). These microstructural and rheological modifications may compromise stiffness and strength of recycled HDPE, even though they often enhance processability. In wood fiber–reinforced composites, the use of recycled matrices has resulted in mixed outcomes, with mechanical performance strongly dependent on the origin and degradation history of the polymer, its blending ratio with virgin resin, and the presence of coupling agents (Olakanmi and Strydom 2016; Isaza *et al.* 2022; Ayana *et al.* 2024). While several studies have addressed the macroscopic behavior of wood–plastic composites containing recycled polyolefins, detailed nanomechanical information on how matrix recycling alters the fiber–matrix interphase remains scarce. This gap motivates the present work, which focuses on directly probing the interface in wood fiber-reinforced composites prepared with virgin and recycled HDPE matrices by nanoindentation.

In fiber-reinforced polymer composites, the interface constitutes a narrow, three-dimensional region between the fiber and matrix where mechanical, physical, and chemical interactions occur. Its structure and properties differ from those of the adjacent phases (Jesson and Watts 2012; Kabir *et al.* 2012; Olakanmi and Strydom 2016; Huang *et al.* 2021; Ayana *et al.* 2024). The interface can be regarded as a third phase, with a thickness ranging from a few nanometers to several micrometers depending on the materials and processing conditions (Kim *et al.* 2001; Cech *et al.* 2013; Islam and Sharif 2015; Le Moigne *et al.* 2018). This size is influenced by multiple factors related to the materials and manufacturing processes and plays a crucial role in the overall performance of the composite material (Nair *et al.* 2010; Charleston *et al.* 2020; Guo *et al.* 2020). The performance of the interface directly affects the stress transfer and distribution, as well as the micromechanical properties between the fiber and the matrix in fiber-reinforced composites, thereby influencing the macromechanical behavior of the material (Zhang *et al.* 2012; Zhu *et al.* 2022). As a result, the structure of the interface in fiber-reinforced composites has gained importance in current studies. The internal mechanical interface, along with associated

failure mechanisms, is considered a critical factor and continues to be a focus of research in materials science (Lu and Youngblood 2015; Dhieb *et al.* 2016; Xu *et al.* 2016; He *et al.* 2020).

The presence of interfaces and their properties play a critical role in composite materials properties and have been extensively validated through studies on fiber-reinforced polymer composites employing synthetic glass and carbon fibers (Gao and Mäder 2002; Cross *et al.* 2005; Molazemhosseini *et al.* 2013; Cicala *et al.* 2017; Enrique *et al.* 2019; Huang *et al.* 2021). The surface morphology and chemical composition of natural fibers exhibit substantial heterogeneity and variability, which significantly complicate the interfacial interactions between natural fibers and the polymer matrix. This inherent complexity poses challenges in accurately characterizing and quantifying these interfaces (Islam and Sharif 2015; Zhu *et al.* 2020). Despite the existing body of research on interfaces in thermoplastic matrices reinforced with natural fibers, a pronounced gap remains in studies focusing on the precise measurement and characterization of interfacial properties in natural fiber-reinforced polymer composite systems (VanLandingham *et al.* 2001; Han *et al.* 2014).

Direct measurement technologies for interface characterization can be divided into two categories based on their underlying principles and the degree of material disruption: destructive and non-destructive methods (Zhu *et al.* 2020). Non-destructive methods include scanning electron microscopy (SEM), atomic force microscopy (AFM), Fourier transform infrared spectroscopy (FTIR), and X-ray photoelectron spectroscopy (XPS). These advanced techniques provide high-resolution images that facilitate the precise identification of interface boundaries between wood and plastic. However, these techniques are generally limited in their ability to directly quantify nanomechanical properties within the interphase region.

Beyond conventional AFM imaging, recent advances in AFM-based nanomechanical mapping, particularly Peak Force Quantitative Nanomechanical Mapping (PF-QNM), have enabled non-destructive, high-resolution quantification of local mechanical properties at the nanoscale. PF-QNM operates by acquiring force distance curves at each pixel, allowing quantitative extraction of modulus, adhesion, deformation, and energy dissipation with spatial resolutions below 10 nm. This approach has been successfully applied to characterize the nanomechanical behavior of plant fiber cell walls, such as flax fibers (Arnould *et al.* 2017), as well as to map interphase regions in carbon fiber-reinforced polymer composites (Qi *et al.* 2019). Despite these advantages, PF-QNM measurements are inherently surface-sensitive and strongly influenced by tip calibration, indentation depth limitations, and substrate effects, which may complicate the interpretation of subsurface or bulk interphase properties. In contrast, instrumented nanoindentation enables depth-controlled probing of localized regions under well-defined loading conditions, allowing the evaluation of nanomechanical properties across fiber, interphase, and matrix regions with greater penetration depth. Accordingly, PF-QNM and nanoindentation should be regarded as complementary techniques rather than competing approaches. In the present study, nanoindentation was selected to characterize the nanomechanical response and thickness of the wood fiber–HDPE interphase, providing depth-resolved mechanical information that complements surface-based AFM techniques.

A technique capable of measuring these properties at the nanometric level is nanoindentation, which is established as a powerful method for mapping and measuring mechanical properties on a nanoscale. It provides detailed information about the hardness and elastic modulus of materials at highly localized levels (Ayana *et al.* 2024). Variations

in mechanical properties can help define the presence and extent of the interface, enabling a deeper understanding of how interface modifications and treatments of individual components influence the overall properties of the composite.

Nanoindentation is a highly effective technique for quantifying mechanical properties at the nanometric scale, making it an indispensable tool for mapping and characterizing material behavior at highly localized levels (Oliver and Pharr 1992; VanLandingham *et al.* 2001; Gindl *et al.* 2006; Lee *et al.* 2007; Tze *et al.* 2007; Xing *et al.* 2009; Wu *et al.* 2010; Zhang *et al.* 2012; Zare *et al.* 2025). However, research on the interfacial properties of lignocellulosic polymer composites using this technique remains limited (Zhou 2018).

Lee *et al.* (2007) and Nair *et al.* (2013) obtained high-resolution images of the elastic modulus distribution within the interface of lyocell fiber/polypropylene composites and, for the first time, identified a small transition region distinct from the reinforced phase and the matrix phase. Additionally, they observed a strong positive correlation between the thickness of this transition region and the macroscopic tensile mechanical properties of the composites. Similarly, Zhu *et al.* (2020) emphasized that despite the small size of the interface phase between plant fibers and thermoplastic polymers, it plays a critical role in influencing the macroscopic mechanical performance of the composite.

Quantitative mechanical measurements of interfaces with a thickness below 1 μm are rarely reported in the literature. In this context, Lee *et al.* (2007) evaluated the interface properties of a polypropylene composite reinforced with natural fibers using nanoindentation and finite element analysis. Although they were unable to directly measure the interfacial layer, their results suggested that its thickness was less than 1 μm.

The limited availability of quantitative data on the mechanical properties of the interface represents a significant barrier to the advancement of natural fiber-reinforced polymer composites. The inherent incompatibility between the hydrophilic natural fiber and the hydrophobic polymer matrix results in the formation of a weak and narrow interface, which adversely affects the composite's performance (Lee *et al.* 2007; Nair *et al.* 2010; Nair 2012).

The *insitu* determination of the mechanical properties of composites using nanoindentation offers a detailed understanding of the interfacial characteristics, enabling a more comprehensive assessment of the overall material properties and facilitating the optimized design of wood-plastic composites (Graham *et al.* 2000; Zhou 2018). The objective of this study was to nanomechanically characterize composite phases in wood-plastic composite and accurately determine the thickness and mechanical properties of the interface using nanoindentation.

EXPERIMENTAL

Materials

Virgin and recycled High-Density Polyethylene (HDPE) in pellet form were used as the polymer matrix. Both types of HDPE were supplied by Plastic Besalle Ltd. (Concepción, Chile). The recycled HDPE consisted of pellets derived from rejected residues generated during the company's plastic bag production process. The material had undergone three extrusion cycles prior to use. Thermal characterization of both matrices was carried out using Differential Scanning Calorimetry (DSC 214 Polyma, NETZSCH-Gerätebau GmbH, Selb, Germany). Measurements were performed in triplicate from 20 °C

to 300 °C at a heating rate of 10 °C min^{-1}. The enthalpy of fusion (mJ g^{-1}) was determined from the area under each endothermic peak. A maleated polyethylene coupling agent (MAPE, Licocene 4351) was supplied by Clariant AG (Frankfurt, Germany). A fine-grain polyethylene wax (Licolub H12; acid value 15 to 19 mg KOH g^{-1}), also obtained from Clariant AG, was used as a lubricant. Radiata pine sawdust used as the lignocellulosic reinforcement was supplied by CMPC Maderas S.A., Coronel Plant (Concepción, Chile).

Preparation of Wood–Plastic Composite Samples

Radiata pine sawdust was sieved, and the fraction retained on a 60-mesh screen (250 μm) was selected for use. The retained particles were oven-dried at 103 ± 2 °C to achieve a moisture content below 2%. Composite processing was carried out using a twin-screw co-rotating extruder (TC35, Cincinnati Milacron, Cincinnati, OH, USA) with a screw diameter of 35 mm, three heating zones, and a rectangular die (50 × 5 mm). The barrel and die temperatures were maintained at 185 and 170 °C, respectively. Two composite formulations were prepared with a wood/plastic ratio of 20/80, using either virgin or recycled HDPE as the polymer matrix. All component ratios are expressed on a weight basis (wt%), corresponding to 20 wt% wood flour and 80 wt% HDPE. This formulation approach was selected to ensure consistency with industrial processing practices and to facilitate comparison with previous studies on wood–plastic composites. In the first extrusion stage, a die equipped with twelve holes was used to produce filaments, which were subsequently pelletized using a milling machine (Model ML-SC-3, Ming Lee Industrial (HK) Limited, Hong Kong, China). The resulting wood-plastic pellets were mixed with the coupling agent and lubricant in a thermal mixer at 80 °C for 5 min. The coupling agent (MAPE) was added at 5% of the oven-dry wood weight, and the lubricant (polyethylene wax) at 1% of the polymer weight.

Thereafter, the two wood plastic formulations were extruded, and composite samples were obtained for characterization. In the first extrusion trial, a die equipped with 12 holes was used to obtain filaments. There were pelletized using a milling machine, (Ming Lee Industrial (HK) Limited, Model ML-SC-3, Hong Kong, China). First, the wood-plastic pellets were mixed with the coupling agent and the lubricating agent in a thermal mixer at a temperature of 80 °C for 5 min. The concentration of the coupling agent was maintained at 5% based on the dry weight of the wood and the lubricating agent at 1% based on the weight of the polymer. Subsequently, the wood plastic composites for the two wood/plastic formulations were incorporated into the extruder and then composites samples to characterization were obtained.

Differential Scanning Calorimetry (DSC)

Differential scanning calorimetry analyses were conducted using a DSC 214 Polyma instrument (NETZSCH-Gerätebau GmbH, Selb, Germany). Approximately 8 to 10 mg of each polymer sample (virgin and recycled HDPE) were sealed in aluminum pans and heated from 30 to 300 °C at a rate of 10 °C min^{-1} under a nitrogen atmosphere (50 mL min^{-1}). The melting temperature (T_m) and crystallization behavior were determined from the endothermic and exothermic peaks, respectively. The degree of crystallinity was calculated according to ASTM D3418-10 (2015), using a reference enthalpy of 293 J g^{-1} for 100% crystalline polyethylene.

Melt Flow Index (MFI)

The melt flow index (MFI) was determined using a CEAST MF20 melt flow indexer (Instron, Norwood, MA, USA) in accordance with ASTM D1238-10 (Condition 190 °C / 21.6 kg). Approximately 5 g of polymer were introduced into the preheated barrel and conditioned for 7 min before applying the test load. The MFI values were expressed in g / 10 min.

Density

The density of the polymer samples was determined using the gravimetric method. Specimens with nominal dimensions of 50 mm × 50 mm × 30 mm were cut from the extruded composite profiles. Their exact dimensions (thickness, width, and length) were measured using a digital caliper (Mitutoyo Corp., Kawasaki, Japan; accuracy ±0.01 mm). The mass of each specimen was recorded with an analytical balance (XS205DU, Mettler Toledo, Greifensee, Switzerland; accuracy ±0.01 mg). Density (ρ) was calculated as the ratio of mass to volume and expressed in g/cm³. Each reported value corresponds to the mean of five replicates.

Tensile Testing

Tensile properties of the extruded wood plastic composites were evaluated to compare the macroscopic elastic modulus with the nanomechanical modulus obtained by nanoindentation. Tests were performed according to ASTM D638 using Type V specimens machined from the extruded profiles. All tests were conducted at 23 ± 2 °C and 50 ± 5% relative humidity. A universal testing machine (5 kN load cell) was operated at a crosshead speed of 5 mm/min. For each formulation (20/80 virgin HDPE and 20/80 recycled HDPE), five replicates were tested, and the tensile modulus was calculated from the initial linear portion of the stress strain curve.

Measurement of Elastic Modulus (E_m) by Nanoindentation

The extruded composites exhibited an average thickness of approximately 5 mm, with mean densities of 883 kg/m³ for WPCs prepared with virgin HDPE and 837 kg/m³ for those prepared with recycled HDPE. Standard mechanical tests were first conducted to compare the macroscopic mechanical properties of the composites with the nanomechanical elastic modulus obtained at the interface. Specimens from both formulations were sectioned into 3 × 3 × 3 mm cubes, and a truncated pyramid with a 1 mm side length on the truncated face was prepared. This geometry ensured that the wood fibers were exposed in cross section and oriented perpendicularly to the indentation load. Thin sections of approximately 250 nm were obtained from the cube surfaces using a rotary microtome (RM2265, Leica Microsystems, Wetzlar, Germany), first employing a glass knife and subsequently a diamond knife, to achieve a smooth surface suitable for nanoindentation. The microtomy process was carried out under dry conditions. No water or lubricants were used during cutting in order to prevent moisture-induced swelling of the wood fibers or softening of the HDPE matrix. Cutting was performed at room temperature, and the resulting surfaces were inspected using the optical microscope integrated into the nanoindenter to ensure the absence of tearing, smearing, or surface deformation prior to indentation.

Prior to nanoindentation testing, the fiber, interphase, and matrix regions were identified using the optical microscope integrated into the nanoindenter. These optical images were used exclusively to guide the positioning of the indentation path across the

fiber–interphase–matrix regions. No AFM imaging or PF-QNM measurements were performed in this study.

Nanoindentation tests were performed on each phase of the composite wood fiber, interface, and matrix using a Hysitron TI 900 nanoindenter (Bruker, Eden Prairie, MN, USA) equipped with a cube corner diamond tip. A nominal maximum load of 100 µN was applied, with eight indentations per phase. Figure 1 illustrates the indentation layout and the representative zones analyzed.

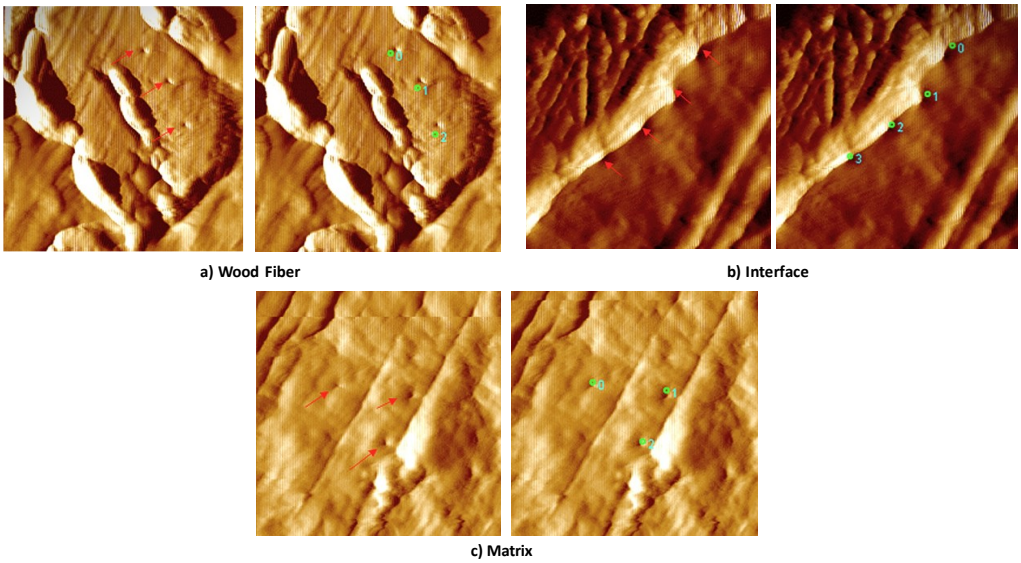

Fig. 1. Optical micrograph acquired using the integrated microscope of the nanoindenter showing the indentation layout across the wood fiber (a), interphase (b), and polymer matrix (c). Red arrows indicate the direction of the linear indentation path, and green points represent representative indentation locations selected for elastic modulus calculation in each phase. The image was used exclusively to guide the positioning of the nanoindentation measurements; no AFM imaging was performed. Approximate field of view: ~20 µm

The indentation cycle consisted of an initial loading period of 5 s to reach the maximum load, followed by a 60 s holding segment at maximum load, and a subsequent unloading period of 5 s. The reduced modulus (E_r) was determined from the load–displacement curve, specifically from the initial unloading slope (S), which represents the elastic response of the material (Fig. 2). The elastic modulus of the sample (E_m) was then calculated using Eq. 1,

$$\frac{1}{E_r} = \frac{1-\nu_m^2}{E_m} + \frac{1-\nu_i^2}{E_i} \quad (1)$$

where E_m and ν_m are the elastic modulus and the Poisson's ratio of indented material, respectively, and E_i and ν_i are the corresponding parameters for the diamond indenter. According to Gacitúa *et al.* (2010) and the Hysitron TI-900 nanoindenter user manual, the following values were assumed: ν_i = 0.07, ν_m = 0.35, and E_i = 1140 GPa. The elastic modulus of the material (E_m) was calculated using Eq. 2.

$$E_m = (1-\nu_m^2)\left(\frac{1}{E_r} - \frac{1-\nu_i^2}{E_i}\right)^{-1} \quad (2)$$

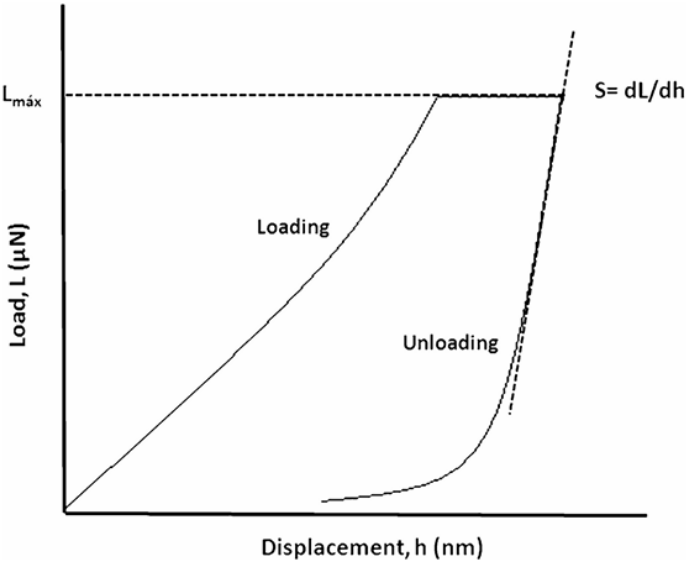

Fig. 2. Load–displacement curve obtained from the nanoindentation test. The initial unloading slope (*S*) was used to calculate the reduced modulus (E_r) (Muñoz *et al.* 2012).

Nanoindentation of the Fiber Matrix Interface

To evaluate both the interphase thickness and the elastic modulus of the composites, a preliminary surface scan was performed using the diamond tip of the nanoindinter. Based on the surface images acquired during tip sample contact, an area was selected in which the three phases wood fiber, interphase region, and polymer matrix were clearly distinguishable. Prior to nanoindentation, these regions were identified using the optical microscope integrated into the nanoindentation system (Hysitron TI 900), which was used exclusively to guide the placement of the indentation path; no AFM imaging was conducted in this study. The optical micrographs acquired with the integrated nanoindenter microscope covered an approximate field of view of ~20 μm, which was sufficient to visualize the narrow fiber–interphase–matrix region characterized in this study. Sequential nanoindentations were subsequently conducted along a linear traverse across the three phases, without predefined spacing between indents, starting from the wood fiber and advancing toward the polymer matrix (Fig. 3). For interphase measurements, indentation points were selected exclusively on continuous solid material. Areas showing visible voids, air gaps, or debonding were avoided. All indentation sites were verified at high magnification to ensure that the tip was positioned over a mechanically continuous region, and any indent displaying non-physical load–displacement behavior was excluded from the analysis.

Statistical Analysis

A general factorial design with a single factor (treatment) and three response variables the elastic modulus of the wood fiber, interface, and matrix was employed. Analysis of variance (ANOVA) was performed at a significance level of $\alpha = 0.05$ using the Design-Expert software package (version 10, Stat-Ease Inc., Minneapolis, MN, USA). Post-hoc comparisons were conducted using a least significant difference (LSD) multiple-range test implemented in Statgraphics (Statgraphics Technologies Inc., The Plains, VA, USA).

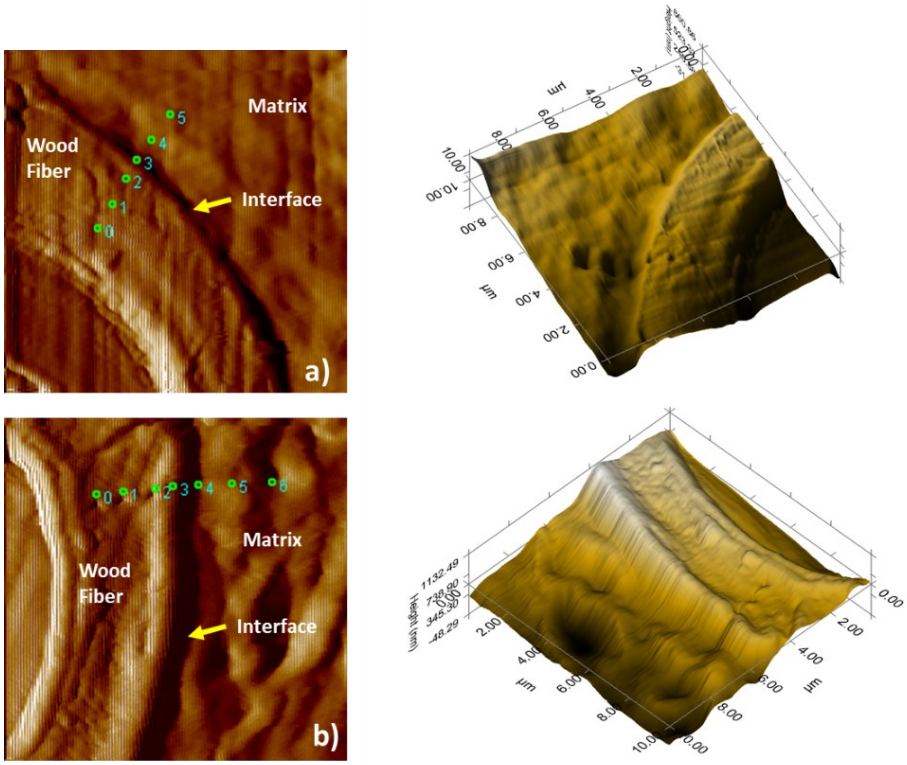

Fig. 3. Optical micrographs obtained with the integrated nanoindenter microscope illustrating the sequential nanoindentation path across the wood fiber–interphase–matrix regions for the two composites: (a) 20/80 virgin HDPE and (b) 20/80 recycled HDPE. The images were used solely for indentation positioning and do not correspond to AFM observations. The indentation sequence follows a linear traverse from the wood fiber toward the polymer matrix. Approximate field of view: ~20 µm

RESULTS AND DISCUSSION

DSC Analysis of the Polymers

Figure 4 presents the DSC thermograms of virgin and recycled HDPE, obtained under identical experimental conditions and over the same temperature range. The melting temperature (T_m) of the virgin HDPE was approximately 136 °C, while the recycled polymer exhibited a slightly lower melting peak at 133 °C. In the case of the recycled HDPE, additional thermal events were observed at higher temperatures: above 180 °C, two exothermic events appeared one of low intensity and another of greater magnitude followed by irregular thermal behavior above 240 °C. These features were not observed, or were negligible, in the DSC thermogram of the virgin HDPE under the same temperature range. The slight reduction in T_m and the presence of these high-temperature exothermic events in the recycled polymer suggest partial chain degradation and a decrease in crystallinity. The reduction likely resulted from multiple extrusion cycles and thermo-mechanical stress during reprocessing. This behavior is consistent with previous studies on recycled HDPE, which report melting peak shifts, peak broadening, and additional thermal phenomena associated with molecular weight reduction and oxidative degradation (Dou and Rodrigue 2021; Langwieser *et al.* 2021; Vidakis *et al.* 2021; Zhang *et al.* 2023).

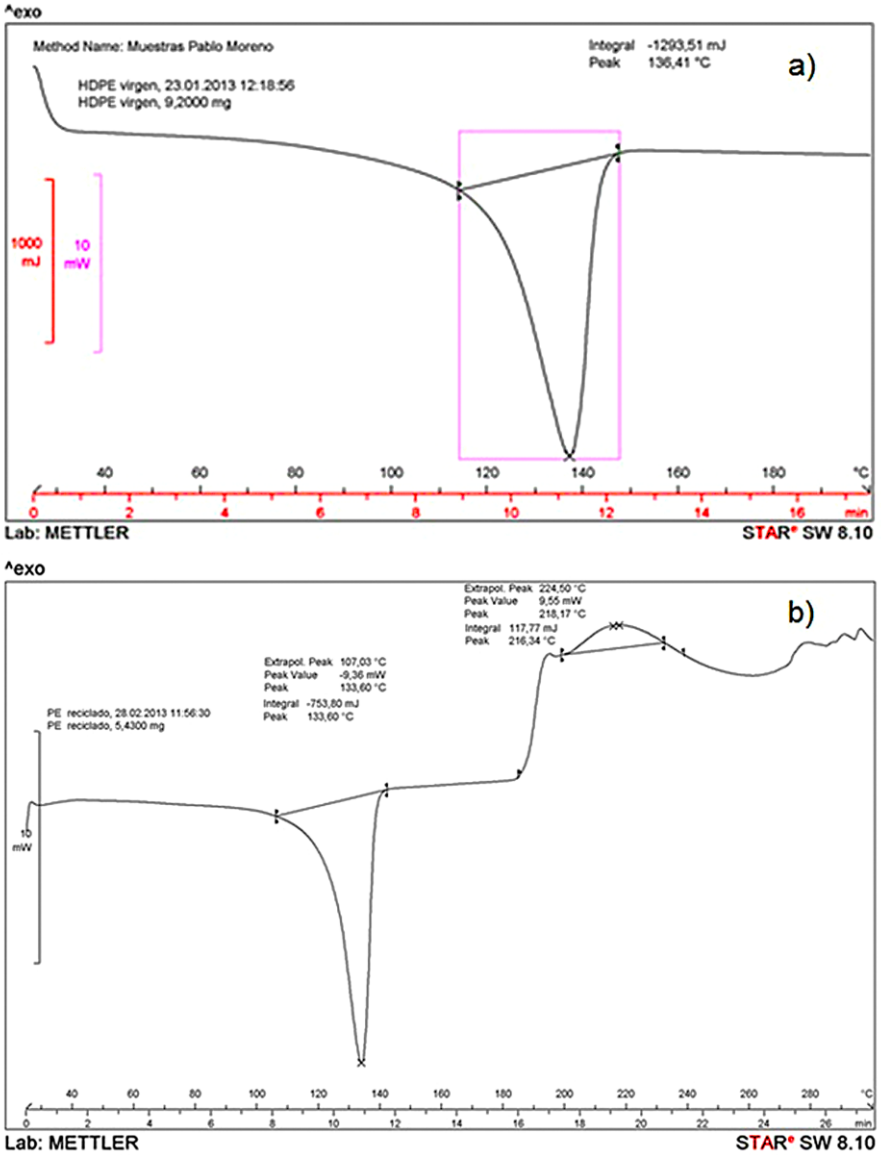

Fig. 4. Differential scanning calorimetry (DSC) thermograms of (a) virgin HDPE and (b) recycled HDPE

Density, Melt Flow Index, and Thermal Behavior of Polymers

The virgin HDPE exhibited a density of 950 kg/m^3, whereas the recycled HDPE had a density of 1112 kg/m^3. The melt flow index (MFI) values were 7.5 g/10 min for the virgin polymer and 13.81 g/10 min for the recycled polymer, as determined according to ASTM D1238 (Condition 190 °C / 21.6 kg).

Differential scanning calorimetry (DSC) analysis revealed distinct differences in the thermal behavior of the two polymers, particularly in their crystallinity and melting temperature. The recycled polymer exhibited a lower degree of crystallinity and a slightly lower melting temperature, which, together with its higher MFI, indicates a more degraded molecular structure resulting from repeated thermal mechanical processing.

This reduction in crystallinity and molecular weight may influence the interfacial adhesion and mechanical performance of the resulting composite potentially decreasing stiffness but improving processability.

Evaluation of the Elastic Modulus of Wood Fibers, Interface, and Matrix

The analysis of variance (ANOVA) results indicated that the model was significant for the elastic modulus response of the three phases in both composites, as the p-value was less than 0.05 (Table 1). The mean comparison test also revealed significant differences in the elastic modulus among the three phases, with higher values observed in the wood fibers, intermediate values for the interface, and lower values for the thermoplastic matrix. This trend was consistent in both composites, as illustrated in Fig. 5. Table 2 summarizes the minimum, maximum, and mean values of the nanoindented elastic modulus obtained for the three phases studied (wood fiber, interface, and matrix).

Table 1. ANOVA Results and p-Value for the Response Variable Elastic Modulus (E_m) and Nanomechanical Properties of Radiata Pine Wood Fiber, Interface, and HDPE Matrix in Extruded Wood Plastic Composites (WPCs)

Composite (Wood/Plastic)	p-value* α=0.05		
	Fiber (GPa)	Interface (GPa)	Matrix (GPa)
20/80 virgin	Model< 0.001	Model < 0.0407	Model < 0.0001
Means	7.51[a]	6.17[b]	2.26[c]
Standard Deviation	0.68	0.92	0.24
Coefficient of Variation (%)	9.06	14.9	10.9
20/80 recycled			
Means	8.16[d]	5.82[e]	1.86[f]
Standard Deviation	0.58	0.76	0.23
Coefficient of Variation (%)	7.19	13.2	12.5
Note: *p-Value < 0.05 indicated that the model was significant; different letters denote a significant difference at a 95% confidence level.			

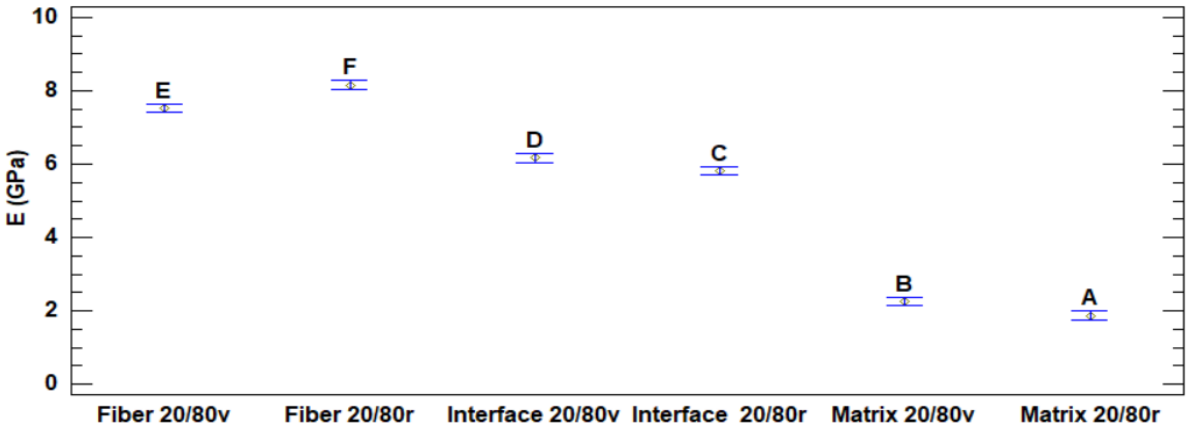

Fig. 5. Comparison of average elastic modulus values across the three phases (fiber, interface, and matrix) for the two compounds. Note: v denotes virgin material and r denotes recycled material

The nanoindentation results, shown in Fig. 6, revealed a continuous variation in the reduced elastic modulus across the fiber, interface, and matrix regions of both 20/80v and 20/80r composites. This gradual transition in mechanical response supports the existence of three distinct microstructural domains, each exhibiting statistically significant differences in modulus values ($p < 0.05$), as confirmed by the least significant difference (LSD) multiple comparison test. The fiber phase exhibited the highest modulus values (7-9 GPa), attributed to the high cellulose crystallinity and the anisotropic multilayered cell

wall structure of lignocellulosic fibers, making it statistically distinct from the other regions. The interface phase showed intermediate modulus values, forming a sigmoidal gradient between the rigid fiber and the ductile matrix, resulting from interdiffusion, mechanical interlocking, and chemical bonding phenomena. Given the inherent incompatibility between HDPE and cellulosic fibers, a sharp mechanical transition would normally be expected at the boundary between the two phases. Without compatibilization, HDPE shows poor wetting of the fiber surface, and no interpenetration of polymer segments is anticipated. Under such conditions, intermediate modulus values measured near the boundary may arise from edge effects rather than representing a true interphase.

In the present study, however, the composites contained 5 wt% MAPE, whose maleic anhydride groups can react with hydroxyl functionalities on the fiber surface while its polyethylene backbone remains miscible with the HDPE matrix. This dual interaction promotes chemical coupling and mechanical continuity along the fiber–matrix boundary. As a result, a more gradual transition in nanoindentation-derived elastic modulus is expected, reflecting a genuine interphase region where polymer chains can partially interpenetrate, entangle, or establish secondary interactions with the fiber surface.

Therefore, the intermediate modulus values observed between the fiber and the matrix likely arise from the MAPE-mediated interphase rather than from measurement artifacts. The improved adhesion produced by MAPE provides a mechanistic explanation for the smoother mechanical gradient detected by nanoindentation across the fiber–matrix boundary.

Its thickness 2.5 µm for 20/80v and 0.63 µm for 20/80r directly influenced the extent of this transition zone. The matrix phase, characterized by the lowest stiffness (1.5-2.5 GPa for virgin HDPE, lower for recycled HDPE), reflected its semicrystalline and ductile nature, with recycled variants exhibiting increased heterogeneity and a reduced modulus due to polymer chain degradation. Each phase was statistically distinguishable based on its elastic behavior.

Table 2. Minimum, Maximum, and Mean Values of the Elastic Modulus (GPa) at the Nanometric Scale for the Three Analyzed Regions: Wood Fiber, Interface, and Matrix

	Wood fiber			Interface			Matrix		
Composite	Min	Max	Mean	Min	Max	Mean	Min	Max	Mean
Wood/plastic 20/80v	6.21	9.93	7.51	4.26	8.94	6.60	1.84	2.80	2.32
Wood/plastic 20/80r	6.44	9.85	8.15	4.01	7.91	5.96	1.51	2.36	1.94

The elastic modulus values obtained by nanoindentation at the interface and within the matrix were higher for the virgin condition of the 20/80 wood plastic composite. In contrast, the fiber modulus was slightly higher in the recycled composite compared with its virgin counterpart. This behavior can be attributed to the heterogeneous cellular structure of radiata pine wood, which alternates between earlywood and latewood regions. The observed variation in fiber modulus may be explained by the nanoindenter tip predominantly interacting with earlywood cells, which generally exhibit lower stiffness than latewood cells. Furthermore, the rigidity of the thermoplastic matrix in the virgin composite may have promoted partial fiber collapse during extrusion, leading to increased fiber compression and agglomeration. These microstructural effects likely contributed to the overall mechanical response of the composite by enhancing interfacial contact and

modifying the load transfer efficiency between phases.

When the elastic modulus values obtained by nanoindentation at the interface regions were compared with those determined from standard tensile tests (20/80v: 1.75 GPa; 20/80r: 1.57 GPa), the nanoindentation derived modulus were, on average, approximately 4.3 times higher than the corresponding tensile test values (Fig. 5).

The differences between the elastic modulus obtained from nanoindentation and tensile testing can be explained by the fundamental contrast in the deformation modes and the scales probed by each technique. Nanoindentation evaluates localized regions with minimal defects under predominantly compressive loading, allowing the intrinsic stiffness of individual phases to be measured. In contrast, tensile testing integrates the response of a much larger volume that includes fibers, matrix, voids, and interfacial imperfections, producing an effective macroscopic modulus. Differences in loading rates and the heterogeneous cellular structure of radiata pine may also contribute to the observed variations. Similar observations have been reported by other authors (Shu and Stanciulescu 2020).

Based on the results, the incorporation of the maleated polyethylene (MAPE) coupling agent at a concentration of 5% significantly enhanced the interfacial adhesion between the polymer matrix and the wood fiber. The functional maleic anhydride groups in MAPE facilitated covalent bonding and strong secondary interactions at the fiber matrix interface, thereby improving compatibility, reducing interfacial defects, and enabling more efficient stress transfer between phases. This enhancement is consistent with previous studies, which reported that the inclusion of maleated coupling agents improves mechanical properties and interfacial bonding in natural fiber reinforced composites through mechanisms dependent on both the concentration and chemical nature of the coupling agent (Lendvai and Patnaik 2022; Khamtree *et al.* 2024; Tongco *et al.* 2025). In the present study, this improved compatibility also resulted in thicker and mechanically more robust interfaces, particularly in the 20/80 virgin WPC formulation, where the highest performance gains were observed.

Several authors (Drzal *et al.* 1983; Guo *et al.* 2020; Shu and Stanciulescu 2020) have emphasized that the structural integrity of composite materials largely depends on the efficiency of stress transfer across the fiber matrix interface, as well as on the intrinsic properties of the constituents and any surface or chemical modifications applied to enhance adhesion. Furthermore, the discrepancy observed between the elastic modulus measured at the macro and nanomechanical scales can be primarily attributed to the sample size effect, as the nanoindentation technique probes localized regions with minimal defects, whereas macroscopic tests integrate the collective behavior of fibers, voids, and interfacial heterogeneities.

The tensile modulus was determined using the effective cross-sectional area of the sample, with the volume subjected to tension being substantially larger than the localized contact area involved in the nanoindentation tests. In addition, the loading rate applied during nanoindentation was typically higher than that used in tensile testing. Whereas tensile testing induced a relatively uniform tensile deformation across the specimen, nanoindentation generated a localized compressive deformation around the indenter. These distinct deformation modes likely accounted for the discrepancies observed in the elastic modulus obtained by the two methods. Similar findings were reported by other authors (Shu and Stanciulescu 2020).

Previous studies have investigated the nanomechanical properties of the fiber–matrix interface in polymer composites reinforced with natural fibers treated with maleated

polypropylene (MAPP) (Nair *et al.* 2013). The reported elastic modulus values of the fibers ranged from 12 to 15 GPa, while the interface exhibited values between 5 and 12 GPa. In comparison, the polymer matrix demonstrated values below 5 GPa, highlighting the distinct mechanical behavior of each composite component. In another study, polypropylene composites reinforced with Lyocell, a regenerated cellulose fiber, were fabricated using silane surface treatments and the incorporation of MAPP (Lee *et al.* 2007). Nanoindentation analysis of the composite phases revealed an elastic modulus of 16.62 GPa for the fiber and 3.03 GPa for the matrix. Similarly, other authors reported matrix elastic modulus values ranging from 2.98 to 3.01 GPa (Jakes *et al.* 2007).

Continuous nanoindentation was employed to evaluate the hardness and elastic modulus of wood cell walls, with reported elastic modulus values for natural wood fibers ranging from 12.7 to 19.3 GPa, depending on the microfibril angle (Tze *et al.* 2007). In a complementary study, the nanomechanical characterization of radiata pine revealed average nanoindented elastic modulus values of the cell walls ranging from 10.49 to 15.02 GPa (Erazo *et al.* 2021). Similarly, nanoindentation was applied to high density polyethylene (HDPE) reinforced with glass fibers, where the elastic modulus of the matrix ranged from 1.45 to 2.75 GPa (Bai 2002).

The elastic modulus values obtained in the present study by nanoindentation for the different phases of the wood plastic composites were consistent with results reported in previous studies. Nevertheless, some variability in the mechanical properties can be expected, as these values are influenced by several factors, including the type of fiber and polymer matrix, the equipment and processing conditions used during composite fabrication, and the specific methodology applied to determine the elastic modulus.

Thickness Interface

Figure 6 presents the elastic modulus profiles obtained by instrumented nanoindentation across the fiber-interface-matrix continuum in the 20/80v and 20/80r composites. A descending gradient was observed, with the fiber phase exhibiting the highest modulus, the interfacial region showing intermediate values with a gradual reduction in stiffness, and the polymer matrix displaying the lowest values. This progressive trend indicated the presence of a mechanically graded interface rather than a sharply defined boundary, suggesting a gradual stress transfer transition zone that enhances interfacial compatibility and load distribution within the composite.

The interface thickness was defined as the region in which the elastic modulus exhibited a continuous and monotonic decrease between the quasi-plateau regions corresponding to the fiber and the matrix. Based on the inflection points of the modulus depth profiles, the 20/80v composite showed a broader interfacial zone with an average thickness of approximately 2.5 μm (2500 nm), whereas the 20/80r composite displayed a considerably narrower interface of 0.63 μm (630 nm).

This difference in interfacial width suggests distinct fiber-matrix interaction mechanisms depending on the polymer type. The broader interface in the virgin HDPE system may be attributed to enhanced polymer wetting, greater molecular interdiffusion, and improved physical or chemical adhesion at the fiber surface. In contrast, the recycled HDPE likely exhibited reduced interfacial compatibility due to oxidative degradation products, lower molecular mobility, and possible surface contamination, all of which could hinder interfacial coupling and reduce stress transfer efficiency.

These results underscore the critical role of the interface in governing local stress transfer mechanisms. A well developed and mechanically graded interfacial region

facilitated efficient load distribution across the constituent phases, thereby enhancing the macroscopic mechanical performance of the composite. Conversely, a reduced or poorly developed interface, as observed in the 20/80r system, may act as a stress concentration site, compromising the structural integrity and reliability of the material under service conditions.

According to the applied methodology, the 20/80v composite exhibited an interface thickness of approximately 2.5 µm (2500 nm), whereas the 20/80r composite showed a markedly thinner interface of about 0.63 µm (630 nm). This thickness was not determined by visual inspection or arbitrary boundary assignment, but was instead derived from the spatial variation of the reduced elastic modulus obtained through high resolution nanoindentation profiling across the fiber-matrix transition zone.

The interface region was defined as the zone in which the elastic modulus exhibited a continuous and monotonic decrease, transitioning from the high modulus characteristic of the fiber to the lower modulus of the polymer matrix. The boundaries of the interfacial region were identified from the inflection points of the modulus distance curve, marking the transition from the fiber plateau to the matrix plateau.

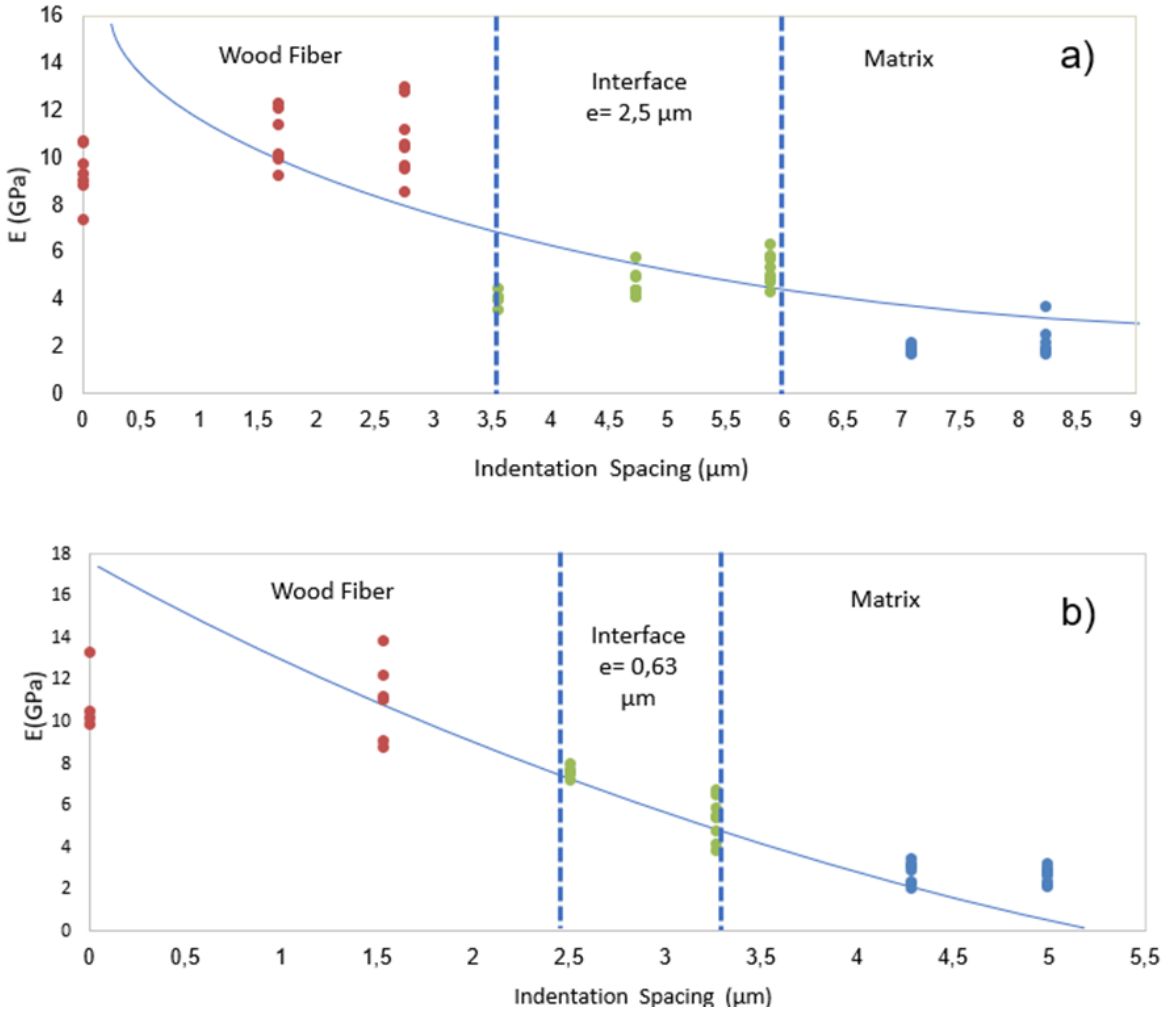

Fig. 6. Elastic modulus profiles and corresponding image analysis showing the interface thickness determined from the modulus gradient in the composites: (a) 20/80 virgin and (b) 20/80 recycled

This approach reflected the mechanically graded nature of the interface, resulting from polymer penetration, interfacial adhesion mechanisms, and stress redistribution near the fiber-matrix boundary. The observed differences in interfacial thickness between the two composites highlighted variations in interfacial interactions.

The broader interface in the 20/80v system may indicate improved polymer wetting and molecular interdiffusion of the virgin HDPE with the fiber surface. In contrast, the thinner interface in the 20/80r composite was likely associated with reduced chain mobility and limited interfacial bonding resulting from thermal oxidative degradation and structural heterogeneity in the recycled polymer.

Interface thicknesses ranging from 31 nm (0.031 μm) to 77 nm (0.077 μm) were reported in natural fiber composites (Nair *et al.* 2013). In glass fiber–reinforced systems, thicknesses between 2 μm (2000 nm) and 6 μm (6000 nm) were observed using nanoindentation and nanoscratching techniques (Hodzic *et al.* 2000). Similarly, values from 1.10 μm (1100 nm) to 8.88 μm (8800 nm) were obtained through atomic force microscopy (AFM) and nanoindentation, with the interface thickness influenced by silane concentration (Cross *et al.* 2005).

In polypropylene composites reinforced with cellulosic fibers, nanoindentation was employed to map the elastic modulus and define the interface thickness from the transitional mechanical properties between fiber and matrix (Lee *et al.* 2007). Consistent with these findings, an average interface thickness of approximately 1.5 μm (1500 nm) was reported for carbon fiber–reinforced epoxy composites using nanoindentation combined with continuous stiffness measurement (CSM) and spatial property mapping (Zhu *et al.* 2022).

The elastic modulus values obtained for the three phases in this study were consistent with those previously reported (Lee *et al*. 2007), which indicated that the thickness of the transition zone was less than 1.6 μm (1600 nm). This value falls within the range of the two experimental measurements obtained in the present work, thereby supporting the reliability and reproducibility of the nanoindentation-based characterization approach.

As previously noted, reports on the mechanical properties of interfaces with widths of 100 nm (0.1 μm) or smaller were limited, primarily due to the lack of techniques capable of measuring properties with nanoscale spatial resolution. It has been emphasized that accurately estimating the effective thickness of the interface using a single indentation profile or a single indentation point within the interfacial region has been particularly challenging (Lee *et al.* 2007; Islam and Sharif 2015). This difficulty has been associated with the potential proximity of the selected zone to the fiber boundary or its partial overlap with the fiber itself (boundary effect), which could lead to inaccurate or nonrepresentative property measurements.

CONCLUSIONS

1. The nanoindentation technique proved to be an effective and reliable method for detecting variations in mechanical properties within the interfacial region of wood polymer composites (WPCs), clearly revealing changes in the elastic modulus along the indentation profile.

2. The incorporation of maleated polyethylene (MAPE) as a coupling agent significantly influenced the nanomechanical response of the composites. The interface thickness measured 2.5 μm in the virgin 20/80 composite and 0.63 μm in the recycled 20/80 composite, in agreement with values reported in previous studies using nanoindentation and atomic force microscopy.
3. The nanomechanical characterization effectively distinguished the three micro-structural phases wood fiber, interface, and matrix. The fiber region exhibited the highest stiffness due to its anisotropic and crystalline structure, whereas the matrix showed the lowest modulus values, reflecting the ductile nature of HDPE.
4. The interfacial region presented intermediate and statistically distinct modulus values, confirming its role as a mechanically graded transition zone responsible for stress transfer between the fiber and matrix.
5. A clear association was observed between the nanomechanical characteristics of the interfacial region and the macroscopic tensile stiffness of the composites. In particular, the broader and mechanically graded interface identified in the virgin HDPE-based composite was associated with more efficient stress transfer between phases.
6. The local mechanical properties of the interfacial region provide useful indicators of composite mechanical behavior and contribute to a better understanding of structure–property relationships in WPCs. However, these observations should be interpreted within the scope of the present experimental dataset and do not imply a direct or universal predictive capability without further systematic investigation.

ACKNOWLEDGMENTS

The authors express their gratitude to the Biomaterials and Nanotechnology Center (CBN) and the Biomass and Bioproducts Valorization Group, both at the Universidad del Bío-Bío, Chile, for their valuable support in the development of this research.

Conflict of Interest

The authors declare that they have no conflict of interest.

Use of Generative AI

During the preparation of this work, the authors used ChatGPT (OpenAI) to assist with writing, translation, and improvement of linguistic clarity in English. After using this tool, the authors reviewed and edited the content as necessary and take full responsibility for the final version of the manuscript.

REFERENCES CITED

ASTM D1238-10 (2010). "Standard test method for melt flow rates of thermoplastics by extrusion plastometer," ASTM International, West Conshohocken, PA.

ASTM D3418-10 (2015). "Standard test method for transition temperatures and enthalpies of fusion and crystallization of polymers by differential scanning calorimetry," ASTM International, West Conshohocken, PA.

Ayana, K. D., Ha, C. S., and Ali, A. Y. (2024). "Comprehensive overview of wood polymer composite: Formulation and technology, properties, interphase modification, and characterization," *Sustainable Materials and Technologies* (40), 1-24. https://doi.org/10.1016/j.susmat.2024.e00983

Bai, S. L. (2002). "Indentation properties of the filler and matrix in polymer composites," *Journal of Materials Science Letters* 21(1), 85-88. https://doi.org/10.1023/A:1014211132219

Beg, M. D. H., and Pickering, K. L. (2008). Reprocessing of wood–fiber reinforced polypropylene composites. Materials & Design, 29(5), 1058–1067. https://doi.org/10.1016/j.compositesa.2008.06.002

Cech, V., Palesch, E., and Lukes, J. (2013). "The glass fiber–polymer matrix interface/interphase characterized by nanoscale imaging techniques," *Composites Science and Technology* (83), 22-26. https://doi.org/10.1016/j.compscitech.2013.04.014

Cestari, S.P., Mendes, L.C., Altstädt, V., Mano, E.B., da Silva, D.F., and Keller, J-H. (2014). "Crystallization kinetics of recycled high-density polyethylene and coffee dregs composites," *Polymers and Polymer Composites* 22(6), 541-550. https://doi.org/10.1177/096739111402200606

Charleston, J., Agrawal, A., and Mirzaeifar, R. (2020). "Effect of interface configuration on the mechanical properties and dislocation mechanisms in metal graphene composites," *Computational Materials Science* 178, 109621. https://doi.org/10.1016/j.commatsci.2020.109621

Cicala, G., Blanco, I., Latteri, A., Ognibene, G., Bottino, F. A., and Fragalá, M. E. (2017). "PES/POSS soluble veils as advanced modifiers for multifunctional fiber reinforced composites," *Polymers* 9(7), 281. https://doi.org/10.3390/polym9070281

Cross, W.M., Cross, W. M., Kjerengtroen, L., and Kellar, J. J. (2005). "Interphase variation in silane-treated glass-fiber-reinforced epoxy composites," *Journal of Adhesion Science and Technology* 19(3-5), 279-290. https://doi.org/10.1163/1568561054352649

Dhieb, H., Buijnsters, J. G., Elleuch, K., and Celis, J. P. (2016). "Effect of relative humidity and full immersion in water on friction, wear and debonding of unidirectional carbon fiber reinforced epoxy under reciprocating sliding," *Composites Part B: Engineering* 88, 240-252. https://doi.org/10.1016/j.compositesb.2015.11.011

Dou, Y., and Rodrigue, D. (2021). "Morphological, thermal, and mechanical properties of recycled HDPE foams *via* rotational molding," *Journal of Cellular Plastics* 58(2), 305-323. https://doi.org/10.1177/0021955X211013793

Drzal, L. T., Rich, M. J., and Lloyd, P. F. (1983). "Adhesion of graphite fibers to epoxy matrices: I. The role of fiber surface treatment," *Journal of Adhesion* 16(1), 1-30. https://doi.org/10.1080/00218468308074901

Enrique-Jimenez, P., Quiles-Díaz, S., Salavagione, H. J., Fernández-Blázquez, J. P., Monclús, M. A., Guzman de Villoria, R., Gómez-Fatou, M. A., Ania, F., and Flores, A. (2019). "Nanoindentation mapping of multiscale composites of graphene-reinforced polypropylene and carbon fibres," *Composites Science and Technology* 169, 151-157. https://doi.org/10.1016/j.compscitech.2018.11.009

Eder, M., Arnould, O., Dunlop, J. W. C., Hornatowska, J., and Salmén, L. (2013). Experimental micromechanical characterisation of wood cell walls. *Wood Science and Technology* 47(1), 163–182. https://doi.org/10.1007/s00226-012-0515-6

Erazo, O., Moreno, P., Valenzuela, P., and Gacitúa, W. (2021). "Propriedades

nanomecânicas de *Pinus radiata* D. Don para uso em productos de alto valor," *Brazilian Journal of Development* 7(11), 109892-109905. https://doi.org/10.34117/bjdv7n11-559

Gacitúa, W., Bahr, D., and Wolcott, M. (2010). "Damage of the cell wall during extrusion and injection molding of wood plastic composites," *Composites Part A: Applied Science and Manufacturing* 41(10), 1454-1460. https://doi.org/10.1016/j.compositesa.2010.06.007

Gao, S. L., and Mäder, E. (2002). "Characterisation of interphase nanoscale property variations in glass fibre reinforced polypropylene and epoxy resin composites," *Composites Part A: Applied Science and Manufacturing* 33, 559-576. https://doi.org/10.1016/S1359-835X(01)00134-8

Gindl, W., Konnerth, J., and Schöberl, T. (2006). "Nanoindentation of regenerated cellulose fibres," *Cellulose* 13(1), 1-7. https://doi.org/10.1007/s10570-005-9017-0

Graham, J. F., McCague, C., Warren, O. L., and Norton, P. R. (2000). "Spatially resolved nanomechanical properties of Kevlar fibers," *Polymer* 41, 4761-4764. https://doi.org/10.1016/S0032-3861(99)00661-8

Guo, R. F., Wang, Y., Shen, P., Shaga, A., Ma, Y. H., and Jiang, Q. C. (2020). "Influence of matrix property and interfacial reaction on the mechanical performance and fracture mechanism of TiC reinforced Al matrix lamellar composites," *Materials Science and Engineering: A* 775, 138956. https://doi.org/10.1016/j.msea.2020.138956

Han, S., Ren, K., Geng, C., Wang, K., Zhang, Q., Chen, F., and Fu, Q. (2014). "Enhanced interfacial adhesion *via* interfacial crystallization between sisal fiber and isotactic polypropylene: Direct evidence from single-fiber fragmentation testing," *Polymer International* 63(4), 646-651. https://doi.org/10.1002/pi.4551

He, M., Xu, P., Zhang, Y., Liu, K., and Yang, X. (2020). "Phthalocyanine nanowires@GO/carbon fiber composites with enhanced interfacial properties and electromagnetic interference shielding performance," *Chemical Engineering Journal* 388, 124255. https://doi.org/10.1016/j.cej.2020.124255

Hodzic, A., Stachurski, Z. H., and Kim, J. K. (2000). "Nano-indentation of polymer–glass interfaces: Part I. Experimental and mechanical analysis," *Polymer* 41, 6895-6905. https://doi.org/10.1016/S0032-3861(99)00890-3

Huang, S., Fu, Q., Yan, L., and Kasal, B. (2021). "Characterization of interfacial properties between fibre and polymer matrix in composite materials: A critical review," *Journal of Materials Research and Technology* 13, 1441-1484. https://doi.org/10.1016/j.jmrt.2021.05.076

Isaza, C. A. V., Yepes, W. U., and Mena, J. (2022). "Mechanical performance of polyolefinic wood plastic composites," *Revista Lasallista de Investigación* 19(1), 265-284. https://doi.org/10.22507/rli.v19n1a16

Islam, M. K., and Sharif, A. (2015). "Nanocharacterization of interface between natural fiber and polymer matrix: An overview," *Composites Interfaces* 23(2), 105-123. https://doi.org/10.1080/09276440.2016.1103082

Jakes, J. E., Hermanson, J. C., and Stone, D. S. (2007). "Nanoindentation of the interphase region of a wood-reinforced polypropylene composite," in: *Proceedings of Ninth International Conference on Wood & Biofiber Plastic Composites*, Madison, WI, USA, pp. 197-205.

Jesson, D. A., and Watts, J. F. (2012). "The interface and interphase in polymer matrix composites: Effect on mechanical properties and methods for identification," *Polymer Reviews* 52 (3-4), 321–354. https://doi.org/10.1080/15583724.2012.710288

Kabir, M. M., Wang, H., Lau, K. T., and Cardona, F. (2012). "Chemical treatments on plant-based natural fibre reinforced polymer composites: An overview," *Composites Part B: Engineering* 43(7), 2883-2892. https://doi.org/10.1016/j.compositesb.2012.04.053

Khamtree, S., Srivabut, C., and Kaewmai, R. (2024). "Effects of natural fiber waste, content, and coupling agent on the physical and mechanical properties of wood species-plastic composites as green materials," *Fibers and Polymers* 25(4), 1391-1402. https://doi.org/10.1007/s12221-024-00493-9

Kim, J. K., Sham, M. L., and Wu, J. (2001). "Nanoscale characterisation of interphase in silane-treated glass fibre composites," *Composites Part A: Applied Science and Manufacturing* 32, 607–618. https://doi.org/10.1016/S1359-835X(00)00163-9

Langwieser, J., Schweighuber, A., Felgel-Farnholz, A., Marschik, C., Buchberger, W., and Fischer, J. (2022). "Determination of the influence of multiple closed recycling loops on the property profile of different polyolefins," *Polymers* 14(2), 2429. https://doi.org/10.3390/polym14122429

Le Moigne, N., Otazaghine, B., Corn, S., Angellier-Coussy, H., and Bergeret, A. (2018). "Characterization of the interface/interphase in natural fibre-based composites," in: *Texbook Surface and Interfaces in Natural Fibre Reinforced Composites*: *Fundamentals, Modifications and Characterization*, Springer International Publishing, Cham, pp. 101-133.

Lee, S. H., Wang, S., Pharr, G. M., and Xu, H. (2007). "Evaluation of interphase properties in a cellulose fiber-reinforced polypropylene composite by nanoindentation and finite element analysis," *Composites Part A: Applied Science and Manufacturing* 38(6), 1517-1524. https://doi.org/10.1016/j.compositesa.2007.01.007

Lendvai, L., and Patnaik, A. (2022). "The effect of coupling agent on the mechanical properties of injection molded polypropylene/wheat straw composites," *Acta Technica Jaurinensis* 15(4), 232-238. https://doi.org/10.14513/actatechjaur.00677

Lu, J. H., and Youngblood, J. P. (2015). "Adhesive bonding of carbon fiber reinforced composite using UV-curing epoxy resin," *Composites Part B: Engineering* 82, 221-225. https://doi.org/10.1016/j.compositesb.2015.08.022

Molazemhosseini, A., Tourani, H., Naimi-Jamal, M. R., and Khavandi, A. (2013). "Nanoindentation and nanoscratching responses of PEEK-based hybrid composites reinforced with short carbon fibers and nano-silica," *Polymer Testing* 32(3), 525-534. https://doi.org/10.1016/j.polymertesting.2013.02.001

Muñoz, F., Valenzuela, P., and Gacitúa, W. (2012). "*Eucalyptus nitens*: Nanomechanical properties of bark and wood fibers," *Applied Physics A*: *Materials Science and Processing* 108(4), 1007-1014. https://doi.org/10.1007/s00339-012-7014-3

Nair, S. S. (2012). *Nanoscale Characterization of Fiber/Matrix Interphase and its Impact on the Performance of Natural Fiber Reinforced Polymer Composites*, Ph.D. Dissertation, University of Tennessee, Knoxville, TN, USA, (https://trace.tennessee.edu/utk_graddiss/1353/).

Nair, S. S., Hurley, D. C., Wang, S., and Young, T. M. (2013). "Nanoscale characterization of interphase properties in maleated polypropylene-treated natural fiber-reinforced polymer composites," *Polymer Engineering and Science* 53(4), 888-896. https://doi.org/10.1002/pen.23330

Nair, S. S., Wang, S., and Hurley, D. C. (2010). "Nanoscale characterization of natural fibers and their composites using contact-resonance force microscopy," *Composites Part A: Applied Science and Manufacturing* 41(5), 624-631.

https://doi.org/10.1016/j.compositesa.2010.01.009
Olakanmi, E. O., and Strydom, M. J. (2016). "Critical materials and processing challenges affecting the interface and functional performance of wood polymer composites (WPCs)," *Materials Chemistry and Physics* 171, 290-302. https://doi.org/10.1016/j.matchemphys.2016.01.020
Oliver, W. C., and Pharr, G. M. (1992). "An improved technique for determining hardness and elastic modulus using load and displacement sensing indentation experiments," *Journal of Materials Research* 7(6), 1564-1583. https://doi.org/10.1557/JMR.1992.1564
Stark, N. M., and Rowlands, R. E. (2003). "Effects of wood fiber characteristics on mechanical properties of wood–polypropylene composites," *Wood and Fiber Science* 35(2), 167–174.
Shu, W., and Stanciulescu, I. (2020). "Shear-lag analysis of capped carbon nanotube reinforced composites with interface damage," *Composite Structures* 242, 112107. https://doi.org/10.1016/j.compstruct.2020.112107
Tongco, J. V. (2025). "Effects of low concentration coupling agent addition on the physicomechanical behavior of wood fiber/HDPE composite," *Mediterranean Journal of Chemistry* 15(2), 187-195. https://doi.org/10.13171/mjc02504301840tongco
Tze, W. T. Y., Wang, S., Rials, T. G., Pharr, G. M., and Kelley, S. S. (2007). "Nanoindentation of wood cell walls: Continuous stiffness and hardness measurements," *Composites Part A: Applied Science and Manufacturing* 38(3), 945-953. https://doi.org/10.1016/j.compositesa.2006.06.018
VanLandingham, M. R., Villarrubia, J. S., Guthrie, W. F., and Meyers, G. F. (2001). "Nanoindentation of polymers: An overview," *Macromolecular Symposia* 167, 15-43. https://doi.org/10.1002/1521-3900(200103)167:1<15::AID-MASY15>3.0.CO;2T
Vidakis, N., Petousis, M., and Maniadi, A. (2021). "Sustainable additive manufacturing: Mechanical response of high-density polyethylene over multiple recycling processes," *Recycling* 6(1), 4. https://doi.org/10.3390/recycling6010004
Wu, Y., Wang, S., Zhou, D., Xing, C., Zhang, Y., and Cai, Z. (2010). "Evaluation of elastic modulus and hardness of crop stalk cell walls by nano-indentation," *Bioresource Technology* 101(8), 2867-2871. https://doi.org/10.1016/j.biortech.2009.10.074
Xing, C., Wang, S., and Pharr, G. M. (2009). "Nanoindentation of juvenile and mature *Pinus taeda* L. wood fibers as affected by thermomechanical refining pressure," *Wood Science and Technology* 43(7-8), 615-625.
Xu, H., Zhang, X., Liu, D., Yan, C., Chen, X., Hui, D., and Zhu, Y. (2016). "Cyclomatrix-type polyphosphazene coating: Improving interfacial property of carbon fiber/epoxy composites and preserving fiber tensile strength," *Composites Part B: Engineering* 93, 244-251. https://doi.org/10.1016/j.compositesb.2016.03.033
Zare Ghomsheh, M., Spieckermann, F., Polt, G., Wilhelm, H., and Zehetbauer, M. (2015). "Analysis of strain bursts during nanoindentation creep of high-density polyethylene," *Polymer International* 64(11), 1537-1543. https://doi.org/10.1002/pi.4967
Zhang, J., Hirschberg, V., and Rodrigue, D. (2023). "Blending recycled high-density polyethylene (rHDPE) with virgin (vHDPE) as an effective approach to improve the mechanical properties," *Recycling* 8(1), 2. https://doi.org/10.3390/recycling8010002
Zhang, T., Bai, S. L., Zhang, Y. F., and Thibaut, B. (2012). "Viscoelastic properties of

wood materials characterized by nanoindentation experiments," *Wood Science and Technology* 46(5), 1003-1016. https://doi.org/10.1007/s00226-011-0458-3

Zhou, Y. (2018). *Interface Optimisation and Bonding Mechanism of Rubber-Wood-Plastic Composites*, Ph.D. Dissertation, Brunel University London, Uxbridge, United Kingdom.

Zhu, J., Lang, F. C., Wang, S. Y., Li, Z., and Xing, Y. M. (2022). "Determination of the interfacial properties of carbon fiber reinforced polymers using nanoindentation," *Journal of Reinforced Plastics and Composites* 41(13-14), 509-516. https://doi.org/10.1177/07316844211063571

Zhu, Z. H., Zhang, Y., Zhang, N., Hao, M. Y., and Wu, H. W. (2020). "Review of the test methods of the interface characterization of natural fiber-reinforced polymer composites," *IOP Conference Series: Series: Materials Science and Engineering* 770 (2020), 012077. https://doi.org/10.1088/1757-899X/770/1/012077

Article submitted: October 24, 2025; Peer review completed: December 1, 2025; Revised version received: January 20, 2026; Accepted: January 30, 2026; Published: February 6, 2026.
DOI: 10.15376/biores.21.2.2980-3001